Dual Monitoring of Surface Reactions in Real-time by Combined Surface-Plasmon Resonance and Field-Effect Transistor Interrogation

Patrik Aspermair[†,‡,§,°], Ulrich Ramach[‡,°], Ciril Reiner-Rozman[†], Stefan Fossati[†], Bernadette Lechner[†], Sergio E. Moya[~], Omar Azzaroni[‖], Jakub Dostalek[†], Sabine Szunerits[§], Wolfgang Knoll[†,‡], Johannes Bintinger[†,*]

[†]: Austrian Institute of Technology, Biosensor Technologies, Konrad-Lorenz-Strasse 24, 3430 Tulln, Austria

[‡]: CEST Competence Center for Electrochemical Surface Technologies, Konrad-Lorenz-Strasse 24, 3430 Tulln, Austria

[~]: CIC biomaGUNE, Paseo Miramon 182 C, 20014 San Sebastian, Spain

[§]: Univ. Lille, CNRS, Centrale Lille, ISEN, Univ. Valenciennes, UMR 8520 - IEMN, 59000 Lille, France

[‖]: Instituto de Investigaciones Fisicoquímicas Teóricas y Aplicadas (INIFTA)−Departamento de Química, Facultad de Ciencias Exactas, Universidad Nacional de La Plata−CONICET, Suc. 4, CC 16, La Plata, Argentina

° Patrik Aspermair and Ulrich Ramach contributed equally.

Table of Contents

I. Theoretical framework

a) Development of the theoretical framework

This chapter aims at a comprehensive evaluation of the electronic EG-FET read-out for LBL assembly. Figure S1 (middle) shows the measurement of the layer-by-layer assembly from the manuscript. Figure S1 (left) shows the corresponding raw data. The baseline correction was performed by linear assumption of a baseline drift and subtraction, resulting in ΔI_{DS}. The resulting ΔI_{DS} after the rinsing steps for each polyelectrolyte layer are shown in Figure S1 (right) to illustrate the stability of the system over 8 layers in a duration of more than 3 hours under continuous flow.

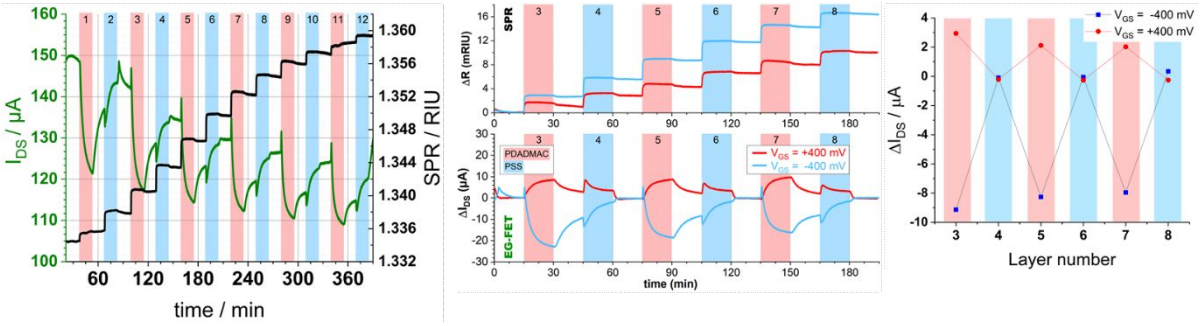

Figure S1. *left*: raw data for -400 mV V_{GS}, *middle*: baseline corrected data of selected layers as shown in Figure 3; *right*: ΔI_{DS} after rinsing of each corresponding PEM extracted from data shown in Figure 3.

A detailed EG-FET and SPR response to the PDADMAC and PSS layer formations are shown in Figure S2. For the fast reactions in this Figure it is important to comment that the rapid responses cannot originate from flow variation due to the peristaltic pump used, as the pump needs about 3-5 min to flush the PEM into the flow cell, thus changing of the pump solution was performed significantly before these observed kinetics.

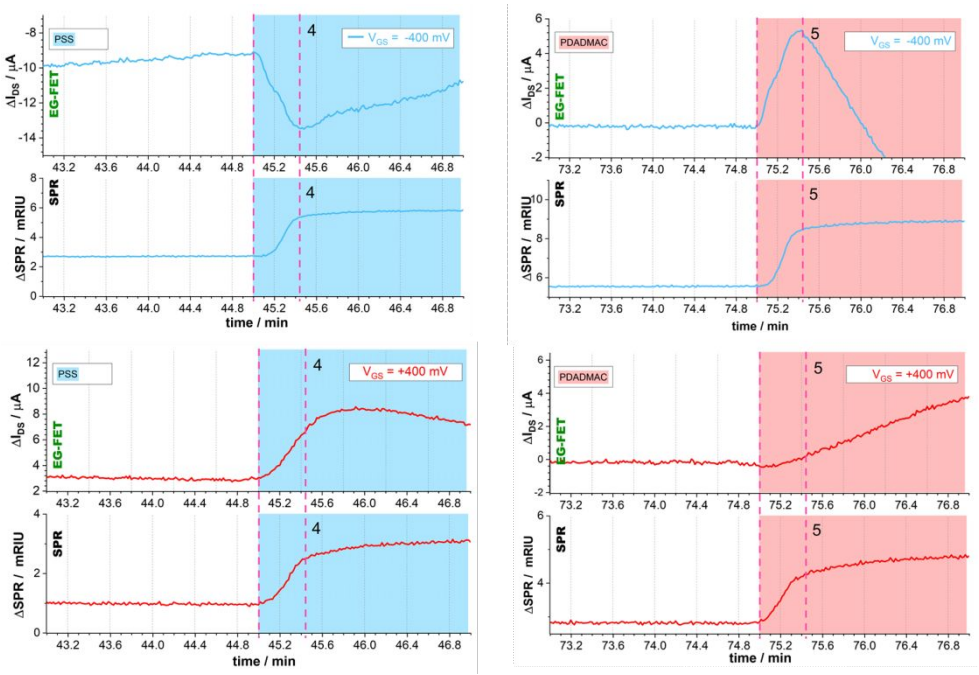

Figure S2. Magnification for the first minutes of each layer deposition from Figure S1 (middle), showing the overlap of two effects both exhibiting exponential behavior with different time constants.

The discussion of the signal obtained from SPR/EG-FET measurements is based on three observations and considerations of sensing mechanisms regarding the sources of the convoluted signal output, which are described in the next section based on the theoretical framework depicted in this section, ascribing the effects to a) bulk changes, b) surface charge accumulation, and c) capacitive effects. For understanding the underlying effects, a few basic formulations and definitions have to be established.

The observed current I_{DS} for the linear region of EG-FET devices can be formulated as:

$$I_{DS} = \frac{W}{L} \; C_i \; \mu \left(V_{GS} - V_T \right) V_{DS} \qquad V_{DS} \ll (V_{GS} - V_T) \qquad \text{(Eq.S1)}$$

Where W is the FET's channel width, L the channel length, C_i the insulating layer capacitance (from Gate to channel), μ is the charge carrier mobility, V_{GS} the applied Gate voltage, V_T the threshold voltage, and V_D the applied voltage between Source and Drain electrodes. Emerging from the basic FET equation (Eq.S1), the time dependency (Eq.S2) of the separate variables is studied in regard to their dependencies to sensing mechanisms.

$$\frac{\partial I_{DS}}{\partial t} = \frac{W}{L} \; \frac{\partial C_i}{\partial t} \; \frac{\partial \mu}{\partial t} \left(V_{GS} - \frac{\partial V_T}{\partial t} \right) V_{DS} \qquad \text{(Eq.S2)}$$

Time dependence of charge carrier mobility $\frac{\partial \mu}{\partial t}$ is the change of charge carrier mobility over time. It depends on several factors, a significant one of those is the effective electric Field, which is described by the Poisson's equation for the effective voltage of the FET channel in the x-coordinate from Gate to channel:[1]

$$F_x = \sqrt{\frac{2}{\varepsilon \varepsilon_r} \int_0^V e \rho(V) \partial V}; \qquad \text{(Eq.S3)}$$

where ε_r is the relative permittivity, ε the absolute permittivity, *e* is unit charge, and ρ(V) is the charge density. Here we also need to introduce the surface charge density σ, which we divide in two components:

$$\sigma = \sigma_i + \sigma_a \qquad \text{(Eq.S4)}$$

where σ_i is the charge density induced to the surface by electric forces and σ_a is the charge density, originating from adsorption of molecules to the surface. Therefore, changes of the surface charge density originating from the electrolyte, namely bulk and capacitive effects, are ascribed to σ_i, while changes of the surface charge potential by direct adsorption of mass are ascribed to σ_a. The Poisson equation clearly shows that the change of surface charge density influences the electric field. On the other hand, it can be understood that similarly also for changes in the electric field, the surface charge density will be modified (the induced part σ_i).

The effective potential at the EG-FET surface by propagation of the electric field is lower than the applied voltage at the gate V_{GS} due to a voltage drop depending on the distance from the electrode and the distribution of dielectric media on the propagation path and can be described by:[1,2]

$$V_{GS,eff} = \frac{Q_{ind}}{C_i} + V_{fb} = \frac{\varepsilon \varepsilon_r F_x(0)}{C_i} + V_{fb} \qquad \text{(Eq.S5)}$$

depending on the flat band voltage V_{fb} which is the difference of the work function of the materials at the interface (Φ_{rGO} - Φ_{KCl}) that can be obtained by electrochemical means, leading to the evaluation of $V_{GS,eff}$ at the surface. The described C_i is the insulator capacitance. For measurements without a gate-electrode (see Figure S4), this part of the equation is 0, therefor $V_{GS,eff} = V_{fb}$. A change of the potential drop at the liquid/solid interface will change $V_{GS,eff}$ and hence the measured signal.

The interface of the electrolyte to the semiconductor with an applied capacitance is described by the **Mott-Schottky** equation:[3]

$$\frac{1}{C^2} = \frac{2}{\varepsilon\,\varepsilon_0 A^2\,q\,N_d}\left(V - V_{fb} - \frac{k_B T}{q}\right) \qquad \text{(Eq.S6)}$$

N_d, the doping density, leads to a change of the FET-mobility due to surface binding of σ and can be obtained from capacitive as well as resistance-based measurements. Doping generally refers to the introduction of impurities into a semiconductor, but in the Mott-Schottky concept it also describes the addition of electrons or holes (by the removal of electrons) into the rGO film.

The indirect way to explain N_d is by describing the surface charge density, which does not take the following parameters into account – e.g. the sign of the charge, the polarity, binding affinity, etc. – but rather offers a very general description of charge distribution and its effect on the EG-FET. Although not all of these parameters regarding the interaction of the polymers with the rGO are known, the relation between doping density and surface charge distribution can still be obtained from Eq.S5, using C_{obs} for determination via the differential capacitance $C = \frac{d\sigma}{d\psi}$, using the surface potential ψ. The surface potential is described by linearization of the Poisson-Boltzmann equation and after rearrangement yields the Debye-Hückel model for the surface charge to surface potential relationship:[4,5]

$$\psi = \frac{\sigma}{\varepsilon\,\varepsilon_0\,\kappa} \qquad \text{(Eq.S7)}$$

which is valid for ionic liquids at interfaces taking into account the Grahame equation for the surface potential distribution, with the reciprocal of κ being the Debye length λ_D:

$$\kappa = \frac{1}{\lambda_D} = \sqrt{\frac{2\,z^2 e^2\,n_0}{\varepsilon\,k_B\,T}}, \qquad \text{(Eq.S8)}$$

where z is the valency of the ions and n_0 is the concentration of ions in an infinite distance from the surface. Also, here the surface charge density is used to describe the surface potential.

The contribution by adsorption which corresponds to σ_a is determined by the introduction of holes *n* or electrons e^- in the rGO-channel. Without V_{GS} the graphene channel current is determined by:[6]

$$I_{DS} = V_{DS} \cdot \frac{W}{L} \cdot n \cdot e^- \cdot \mu_{eff} \qquad \text{(Eq.S9)}$$

where the mobility is governed by Matthiessen's rule: $\mu_{eff} = (\mu_{lattice}^{-1} + \mu_{impurity}^{-1} + \mu_{adsorption}^{-1})$ showing that the response signal is defined by lattice and doping parameters as well as the introduction of charge carriers.

In summary, the mobility, defined by these variables $(\psi, \rho, \sigma, V_{GS,eff}, \mu_{adsorption})$, is related to the charge density by Eq.S10.

The **time-dependence of the mobility** can be described as:[1]

$$\frac{\partial \mu}{\partial t} = \frac{\partial \alpha_\rho / \partial t}{e\,\rho} \qquad \text{(Eq.S10)},$$

with ρ being the charge density and α_ρ the conductivity for a certain ρ.

Relating these observations to the approach to describe the surface charge density via $\sigma = \sigma_i + \sigma_a$, we can conclude that the mobility is determined by both the induced and the adsorbed surface charge. The charge carrier mobility in the EG-FET channel is determined by the change of

conductivity (measured by I_{DS}) in the transistor and is directly given by the dependency of surface charge densities to the applied electric field:

$$\mu = \frac{1}{\rho_i e} \frac{d\sigma}{dV_{GS}} \qquad \text{(Eq.S11)},$$

where ρ_i is the induced charge carrier density at V_{GS} = 1V.

Time dependence of threshold voltage $\frac{\partial V_T}{\partial t}$

For the threshold voltage the time dependence originates from changes in the semiconductor material and from the applied potential. V_T is usually obtained by linear fits of the $I_{DS}V_{GS}$ transfer characteristics; for p- or n-type FETs it is the voltage at which the semiconductor is responding to V_{GS}. This comes from the intrinsic semiconductor and dielectric properties modulated by μ and C_i and are therefore included in the parts above and below. For reduced graphene oxide, which is exerts ambipolar behavior of the transfer characteristics, V_T is not considered as a separate physical quantity, rather than a measured factor used for qualitative determination of I_{DS} from the transfer characteristics and will not be considered independently in this discussion.

Time dependence of capacitance $\frac{\partial C_i}{\partial t}$

Changes of capacitance over time will be evaluated in this section. The capacitance is defined by:

$$Q = C \cdot U \qquad \text{(Eq.S12)},$$

giving the general dependency of charges Q to the applied voltage U (for the FET this is V_{GS}). For a certain geometry of a parallel plated capacitor with the use of a classical dielectrics, the capacitance can be calculated by the distance d between the plates (here the rGO and gate-electrodes), the area A and the dielectric permittivity ε:

$$C = \varepsilon_0 \, \varepsilon_r \, \frac{A}{d} \qquad \text{(Eq.S13)}$$

Since the Applied V_{GS}, the thickness and area of the system are constant during measurements, capacitive changes of the system can originate only from variations in permittivity ε_r or the surface charge σ. In our theoretical framework we assume ε_r of the system constant at any given time during layer deposition. The adsorbed surface charge σ_a leads to a minute change of the capacitance, which is then constant after mass adsorption (as seen from SPR). For the induced surface charge density σ_i, the time-dependent capacitance is given by the differential capacitance as described in electrochemistry by:

$$C = \frac{\partial \sigma}{\partial \psi} \qquad \text{(Eq.S14)},$$

where C, σ and ψ are capacitance, surface charge and electric surface potential.

As shown in Eq.S7, the capacitance only has a time-dependence if the permittivity ε_r and/or the Debye length λ_D vary. Capacitive effects play a crucial role in EG-FET configurated biosensors and in literature are often used as the

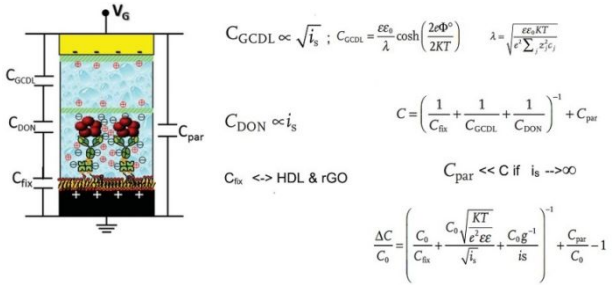

Figure S3. Schematic illustration of the capacitive sensing approach, splitting the system capacitance into serial terms regarding the layers. The dependencies on the ionic strength are shown on the right side.[11]

primary source of the signal, the so called capacitive sensing (Torsi et al)[7]. It has been demonstrated that capacitive sensing does not suffer from Debye-screening limitations[8] and coupled with advanced surface modification principles can lead to the enhancement of the biosensor signal, even down to the single molecule detection level.[9]

A good description for the capacitive effects was given by the Torsi group and concludes a strong dependency of the EG-FET signal to the ionic strength of the buffer solution and the charges originating from the donation layer,[10,11] which in their case is a biomolecule-functionalized architecture, while for a LbL approach with polyelectrolytes it is also the polymeric layer and the thereby induced screening charge ions. The dependencies are shown in Figure S3 (modified from the Torsi group).[11] The effects originating from capacitive sensing can, for simplification, also be described by their influence on the channel material solely, deriving an expression from Ohm's law:

$$j_{DS} = \sigma F \qquad \text{(Eq.S15)}$$

where j_{DS} is the drain current density and F the field from source to drain. Furthermore, we ascribe the capacitive effects to modulations of the channel via the integral of induced surface charge density:[12]

$$I_{DS} = -WdL \int_{V_{GS}}^{V_{GS}-V_{DS}} \sigma(V)\, dV \qquad \text{(Eq.S16)}$$

With d being the thickness of the polymer film. As shown in the chapter for charge carrier mobility, C_i influences the mobility of the rGO layer and can therefore be used as the measuring quantity in the proper system configuration.

Relating these observations to the approach for the surface charge density $\sigma = \sigma_i + \sigma_a$, we can conclude that the capacitance, in contrast to the mobility, varies by the induced surface charge and does not change after each layer deposition, once adsorbed surface charge σ_a is established on the layer.

b) Implementation of the theory for explanation of the experimental results

Using the insights from the previous section we now want to focus on the outcome from the EG-FET/SPR system for LbL deposition as shown in the main article and Figure S1. This section will focus on the effects of a) bulk changes, b) adhered surface charge density σ_a and c) capacitive effects influencing the induced surface charge density σ_i.

• Bulk changes

One Monomer of each polyelectrolyte has one charge (1eV). For PDADMAC, a monomer has 160 g/mol of molecular weight, the polymer has an average weight of 100 kDa. Therefore, 1 mg/ml of PDADMAC in 100 mM KCl as used in the experiment has a monomer concentration of 625 µM, which equals 60.2 Coulomb for a liter of solution. The sensing area of the cell hast a volume of 5 µL, so 300 µC of charge should be introduced into the system at any given time. The ionic strength of the KCl buffer with PDADMAC is 100.625 mM in comparison to 100 mM for the washing steps, a difference of less than one percent.

For PSS, a monomer has 206 g/mol of molecular weight, whereas the polymer has an average weight less or equal than 70 kDa. Therefore, 1 mg/ml of PSS in 100 mM KCl has a monomer concentration of 475 µM, which equals 47.75 Coulomb for a liter of the solution. The sensing area of the cell hast a volume of 5 µL, so 238 µC of charge should be introduced into the system at any given time. The ionic strength of the KCl buffer with PSS is 100.475 mM in comparison to 100 mM for the washing steps, a difference of less than one percent.

This yields changes in ionic strength of about 0.5%, which has a minute effect on the capacitive behavior of the system and the gating effect of the transistor. In relation to the signals obtained during sensing, bulk effects can therefore be neglected.

- ## Surface charge accumulation (σ_a)

The current I_{DS} is determined by the resistance of the channel which is inversely connected to the mobility of the transistor material (here rGO) by Ohm's law:[13]

$$R = \frac{1}{\mu \ C_i \frac{W}{L}(V_{GS} - V_T)} \qquad \text{(Eq.S17)}$$

This holds true because I_{DS} is generated by flow through the transistor layer and not through the applied polymeric layers (R > 1 MΩ for both polyelectrolytes), a resistance several order of magnitude higher than the conducting material. Therefore, polyelectrolyte conductivity can be neglected.

The basic sensing principle for reduced graphene oxide (rGO) biosensors is based on binding or adsorption of analytes to the rGO surface or to the biorecognition units functionalized on the rGO. The principle of such direct sensors is in use, e.g. in graphene based chemiresistors[14] or EG-FETs.
To conduct zero-capacitance measurements our simultaneous SPR/EG-FET setup could not be used, as a gold substrate, which again would introduce capacitive effects, is required for SPR measurements.
Thus, the zero-capacitance measurement setup consists of a two-terminal configuration in which the gate-material was changed from an Au-coated glass slide to a non-coated glass-slide. As the gate was left floating the capacitance is also 0. The results from the measurement are shown in Figure S4. For PDADMAC adsorption and the corresponding washing step the EG-FET signal from the zero-capacitance experiment is in good agreement with the signal from SPR in the standard configuration (Figure S1). In contrast, while PSS adsorption can hardly be observed from the EG-FET signal in the zero-capacitance experiment the post-PSS rinsing steps can again be readily measured. We speculate that this effect for PSS is ascribed to repulsion of PSS from the surface, because the intrinsic negative charge of rGO (like PSS).[15]

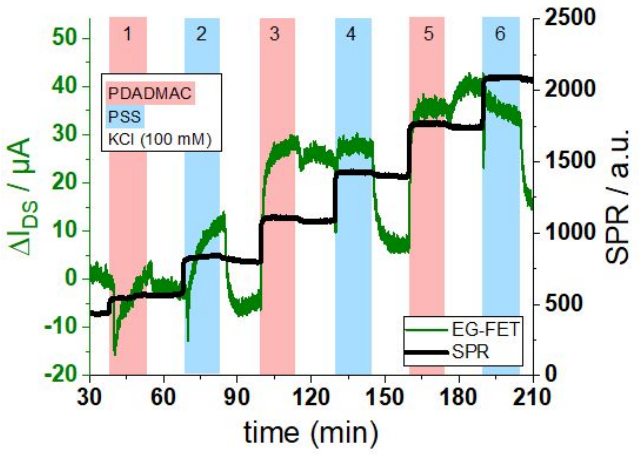

Figure S4. zero-capacitance EG-FET response realized by replacing the gate-electrode with a non-conductive substrate, thus leading to $\sigma = \sigma_a$, comparable with the SPR response from Figure S1.

Exponential fits for the adsorption time constants (t_{on}) of SPR and EG-FET responses for polyelectrolytes, have been evaluated. Obtained time constants are shown in Figure S6.

The difference in the time constants for SPR and zero-capacitance EG-FET (two terminal configuration) signals are due to non-existing applied gate voltage (floating gate) and are shown in Figure S6. The lack of applied voltage changes the surface potential and, as shown in Eq.S5 and Eq.S6, also the affinity to the surface and mobility of the rGO. Furthermore, the time kinetics for additional layers of the applied

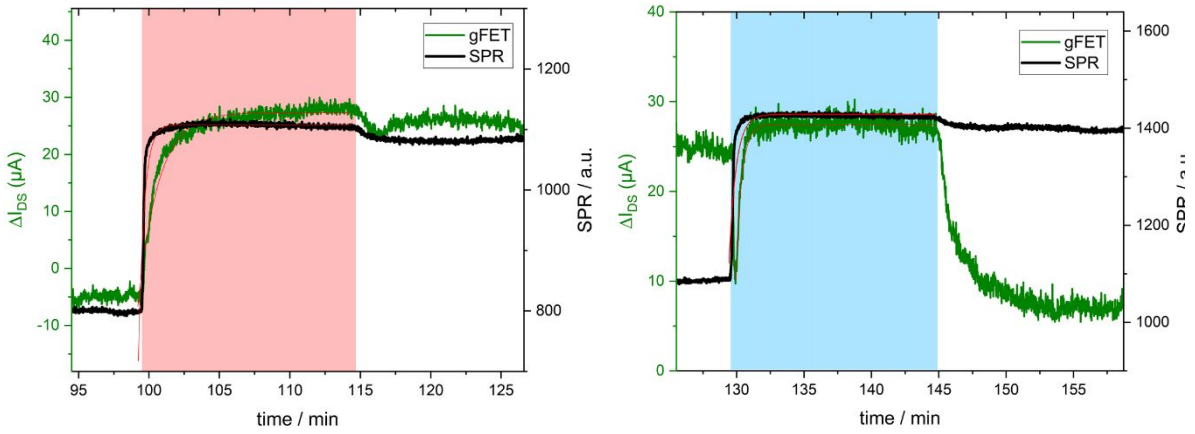

Figure S5. Comparison of the EG-FET responses (green) in a non-capacitive setup with the responses from the SPR signal (black). *left*: shows the third layer, PDADMAC and *right*: shows the fourth layer, PSS

polyelectrolytes converge towards the signals obtained by SPR with increasing number of layers.

The discrepancy between initial layers and later deposited layers can be attributed due to incomplete layer formation for seed layers.

Strikingly, a much better agreement for the time constants obtained from zero-capacitance measurements to SPR (Figure S6) is observed than for time constants from the combined SPR/EG-FET system (Figures S1 and S2). As a result, we conclude that responses obtained from zero-capacitive measurement are attributed to the adsorbed surface charge density σ_a (Eq.S4).

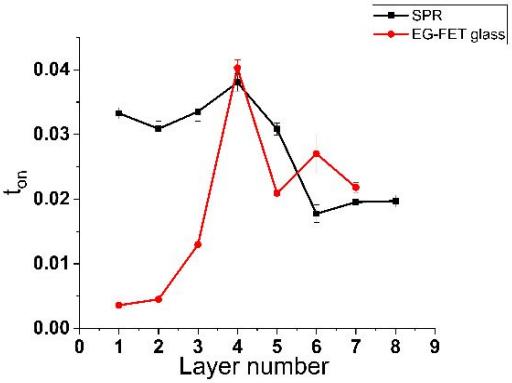

Figure S6. obtained time constants t_{on} from the exp. Fits of the zero-capacitance measurement

- Influence of gate-surface distance

To further support these claims, the flow-cell gasket thickness was increased by a factor of 10, thereby decreasing the overall capacitance of the system (Eq.S13) by the same factor.
It was shown that the capacitive effects are diminished, the measurement is similar to the results obtained by using a non-conductive Gate-electrode (Figure S4). Albeit the capacitive effect still plays a minute roll in this measurement, the advantage of simultaneous SPR measurement, yields a direct comparison of the binding constants shown in Figure S7b. The flow channel thickness is defined by the height of the gasket between the gold slide (gate electrode) and the drain-source electrodes.

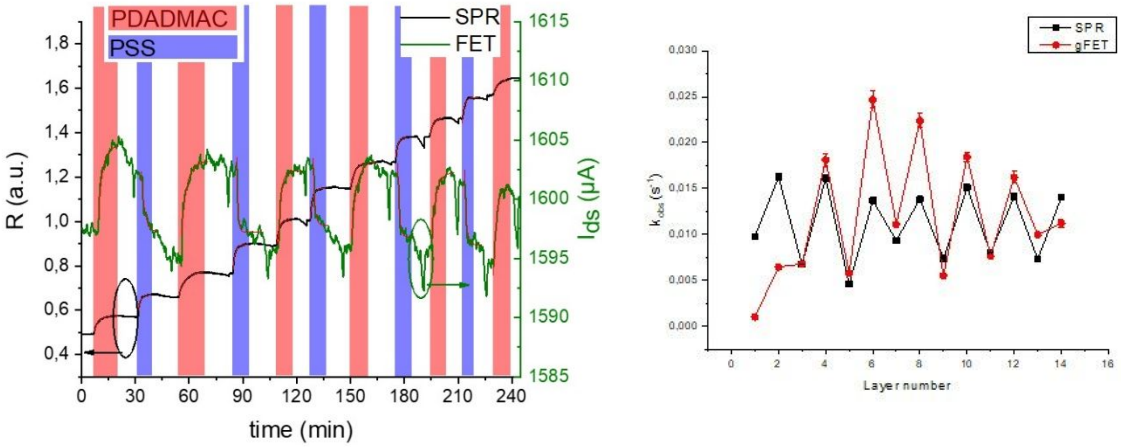

Figure S7. *left*:LbL measurement of SPR/EG-FET with a gasket of 3mm thickness. *right*:time-constants of the exponential fits evaluated form SPR and EG-FET measurements (*left*)in a).

Figure S7b demonstrates that the time constants of this architecture are in good agreement to the time constants obtained from SPR measurements. Therefore, according to Eq.S4, decreasing the capacitance enables the observation of the adsorbed surface charge density, as the term σ_i, induced surface charge density, converges to 0, and results in comparable time constants between EG-FET and SPR readouts.

- Capacitive (σi)

The induced surface charge density σ_i can be obtained by the subtraction of the adsorbed surface charge density σ_a from the total surface charge density σ, as proposed in Eq.S4. Therefore, the measurement in Figure S4 was subtracted from the submitted measurement in Figure S1 with equivalence factors for normalization of 1,4 for PDADMAC (L5) and 2,9 for PSS (L4), to compensate the differences in sensor fabrication, shown in Figure S8.

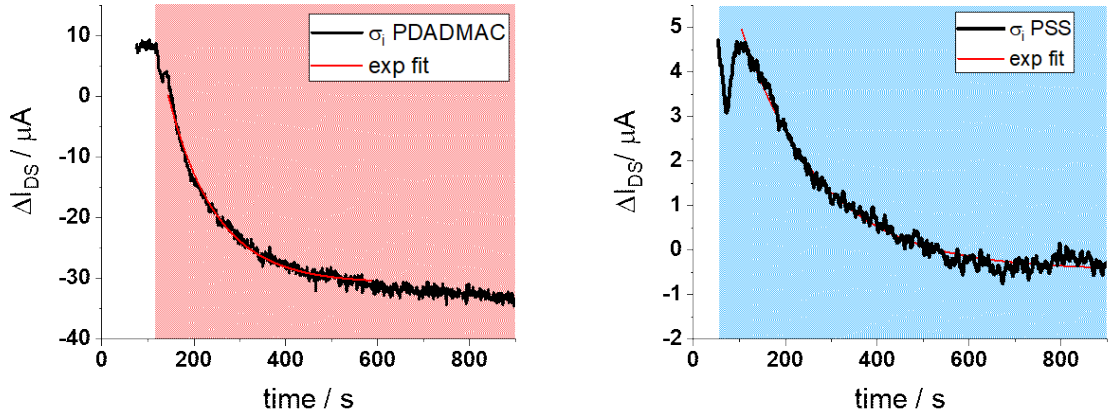

Figure S8. *left*: Subtracted EG-FET response curve for PDADMAC layer deposition and *right*: subtracted response curve for PSS layer deposition.

Slow responses are directly related to ion diffusion in PEM, as discussed in Figure S4: σ_i

As argumentized in the main manuscript the slow responses, for which we demonstrated their origin by the zero-capacitance experiment in the previous section to σ_i, are directly connected to ion diffusion in the PEM layers. To evaluate the tendency for ion diffusion of the separate layers at different V_G we introduced an arbitrary kinetic ratio ξ which is obtained by exponential fitting of the response signals obtained by the subtracted data shown in Figure S8, eliminating the influence of σ_a with the corresponding wash-off kinetics.

We defined this ratio by: $\xi = {t_{on}}/{t_{off}}$, where t_{on} is the time constant in the fit from Figure S8 and t_{off} is the time constant from the corresponding wash-off step. The full fitting data is found in Table S1.

Table S1. t_{on} and t_{off} values for PDADMAC and PSS for positive and negative gate voltage V_{GS}

	PSS		PDADMAC	
(s^{-1})	+ 400mV	- 400mV	+ 400mV	- 400mV
L3 t_{on}			0.0044	0.0049
L3 t_{off}			0.0035	0.0031
L4 t_{on}	0.0055	0.0040		
L4 t_{off}	0.015	0.016		
L5 t_{on}			0.0051	0.0058
L5 t_{off}			0.0035	0.0032
L6 t_{on}	0.0047	0.0039		
L6 t_{off}	0.016	0.020		
L7 t_{on}			0.0052	0.0051
L7 t_{off}			0.0037	0.0038
L8 t_{on}	0.0037	0.0039		
L8 t_{off}	0.017	0.013		

Furthermore, the charge carrier density at the channel-electrolyte interface Q(V) in the accumulation regime of the semiconductor ($V<V_{fb}$). Can then be calculated by:

$$Q(V) = -\int_{-V_{fb}}^{V} C(V)\,\partial V \qquad \text{(Eq.S18)},$$

as demonstrated by the Berggren group.[16]

Such evaluations for charge distribution and similar studies also for diffusion processes not obtained by EG-FET platforms where until now, but always by means of electrochemistry (CV or EIS). However, the suitability of EG-FET systems as complementary tools for electrochemistry has been proposed before.[17] The discussed quantities can also be described by the chemical potential, which in turn is related to the surface potential at a solid/electrolyte interface. For single ion species this thermodynamic approach leads to:[18]

$$\overline{\mu_i} = \mu_i^0 + [\frac{R\,z_i q}{k_B}(\psi_2 - \psi_1)] + z_i q\,\psi \qquad \text{(Eq.S19)},$$

where μ_i^0 is the chemical standard potential, R the molar gas constant, ψ_1 the potential at the solid interface, ψ_2 the potential at the liquid interface. This demonstrates that the applied theoretical framework could also be reformulated using the chemical potentials throughout the system rather than the surface potentials and charge density, which could be a useful mean for the description of more complex chemical experiments performed by the EG-FET/SPR setup where the charge of the analytes is not sufficient for a comprehensive explanation and the chemical activity has to be considered thoroughly. The concept itself is visualized in Figure S9.

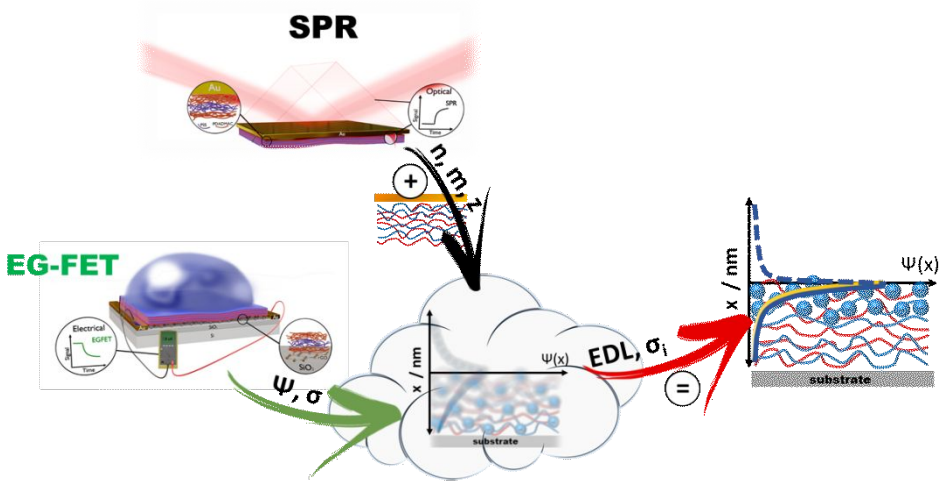

Figure S9. Concept of the EG-FET and SPR signal fusion to obtain a detailed information about the surface charge density. Superimposed surface phenomena can be separated by the simultaneous real-time observation with a bifunctional sensor and the subsequent demodulation.

II. Complementary experiments

This chapter describes additional experiments an illustrates different data representations to justify the developed theoretical framework on the EG-FET/SPR system.

The experiments were performed using a constant flow rate of 100 µl/min and 1 mg/ml PDADMAC and PSS concentrations in 0.1 M KCl electrolyte solutions. All EG-FET experiments were performed at V_{DS} = 0.05 V using the same PDADMAC/PSS solutions as for SPR measurements.

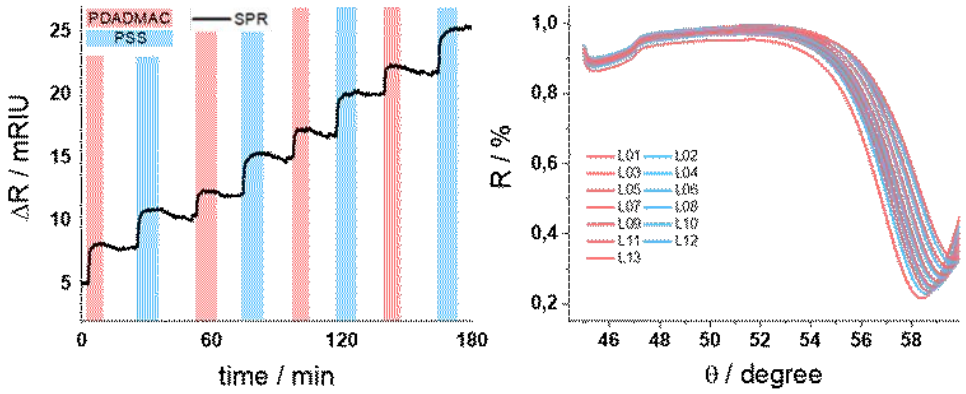

Figure S10. LBL SPR investigations, *left*: kinetic measurement in SPR flow cell using 20 mM KCl and a concentration of 1 mg/ml of PDADMAC and PSS solutions, *right*: corresponding angular scans and the shift of the resonance angle after the completed layer deposition.

Results for measurements with 20mM KCl are shown in Figure S10. To promote LbL assembly the gold surface was activated by UV/ozone treatment beforehand. The intial separated EG-FET experiments were carried out in a flowcell with an Ag/AgCl wire as gating electrode. For the EG-FET/SPR approach, the gating electrode was replaced by the SPR Au-slide with 2 nm Cr adhesion layer and 50 nm Au layer. All kinetic SPR sensor measurements were calibrated with standard glucose solutions to relate the observed changes in SPR reflectivity to refractive index variations.

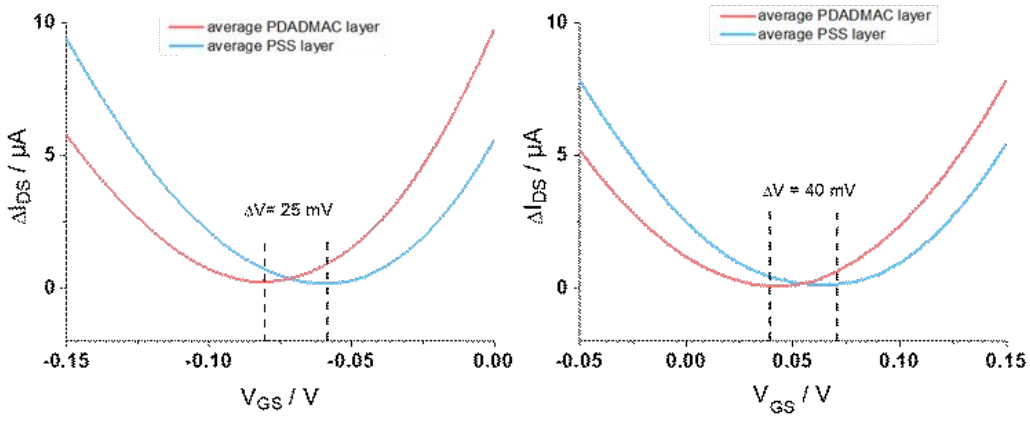

Figure S11. Influence of different ionic strength solutions on the $I_{DS}V_{GS}$ output curves. *left*: $I_{DS}V_{GS}$ measurement in 20 mM KCl using a 1 mg/ml PDADMAC/PSS solution, *right*: $I_{DS}V_{GS}$ measurements in 500 mM KCl electrolyte solution using a 1mg/ml PDADMAC/PSS solution. The Dirac point shift V_i corresponds to the ionic strength of the electrolyte solution.

Dirac points are the minimum of the drain source current I_{DS} and are represented as an average of several $I_{DS}V_{GS}$ scans after each layer deposition. The resulting Dirac shift is a result of the effective electrostatic gating caused by differently charged polyelectrolytes and depends on the ionic strength of the electrolyte solution, shown in Figure S11. The effect of ionic strength on SPR data, which influences the layer thickness, is shown in Figure S12.

- ## Different deposition rates at positive and negative applied potentials:

Figure S12 shows the different PEM growth rates for positive and negative applied gate potentials. It has been previously shown in literature that the rate of deposition of the PEM can be controlled via the application of an external electric field. This effect is observed below voltages which would lead to electrolysis of water, for higher voltages the contribution of electrolysis is dominant.

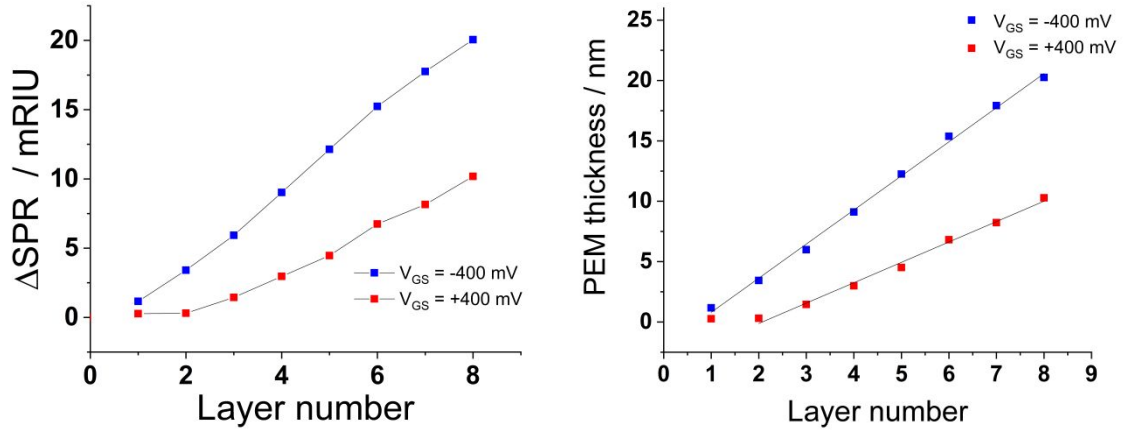

Figure S12. *left*: SPR response to the LbL growth at different applied gate voltages, *right*: PEM layer growth at different applied gate voltages V_{GS}, including a linear fit.

For V_{GS} = +/- 400 mV electrolysis of water only plays a minute role. The polarizability of charged polymers is much higher than water at such low potentials, the polymer chains exhibit instantaneous response to the electrostatic attraction by V_{GS}.[19] Hence, electrophoretic deposition occurs and the electrostatic compensation process between cationic and anionic polyelectrolytes is stronger, resulting in thicker films as seen by the SPR signals which can be seen in Figure S12. Since the same potential strength with different signum was applied for our experiment, the difference of both measurements can therefore be explained by the different polarizability of PDADMAC and PSS at positive and negative potentials. The mean layer growth d_p for the applied gate voltage V_{GS} = -400 mV is 2,82 ±0,06 nm and for V_{GS} = +400 mV is 1,69 ±0,06 nm according to Eq.1 and the accumulating layers are plotted in Figure S12 (right).

Figure S13 shows the raw data including leakage current of the combined EG-FET/SPR measurement in one measurement chamber at simultaneous data acquisition. As can be seen, the leakage current is several orders of magnitude smaller than the electric response signal. We deem it therefore to be neglectable.

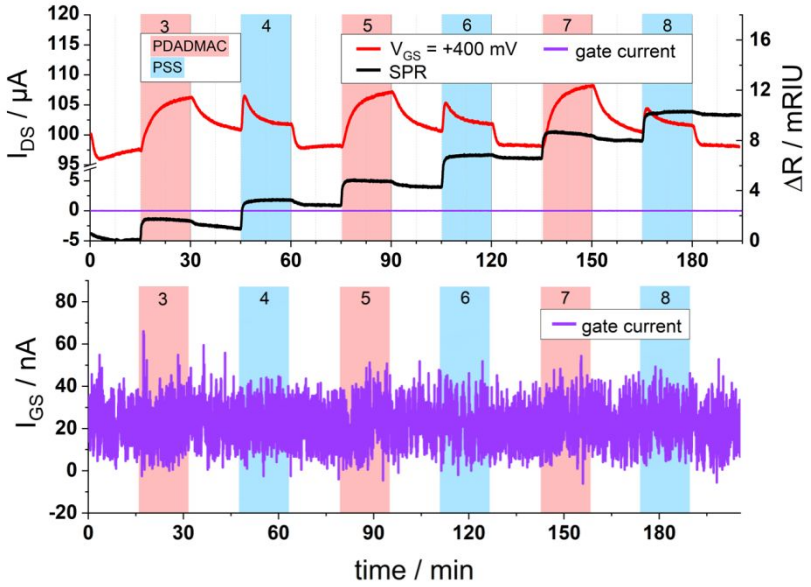

Figure S13. *top*: Raw data of the SPR/EG-FET measurement including leakage current (gate current). *bottom*: Zoom in of the leakage current. EG-FET chips have a leakage current in the order of ~0.02% of the total measured current thus making leakage current irrelevant for measurements.

The I_{DS} shifts at a fixed gate voltage V_{GS} are in accordance with the change in $I_{DS}V_{GS}$-curves due to the adsorption of PEM layers, which is visualized in Figure S14. The deposition of a PSS layer leads to a right shift of the Dirac point V_i, causing an increase of the current I_{DS}, if the working point is adjusted via the gate voltage V_{GS} to a negative slope along the transfer characteristic.

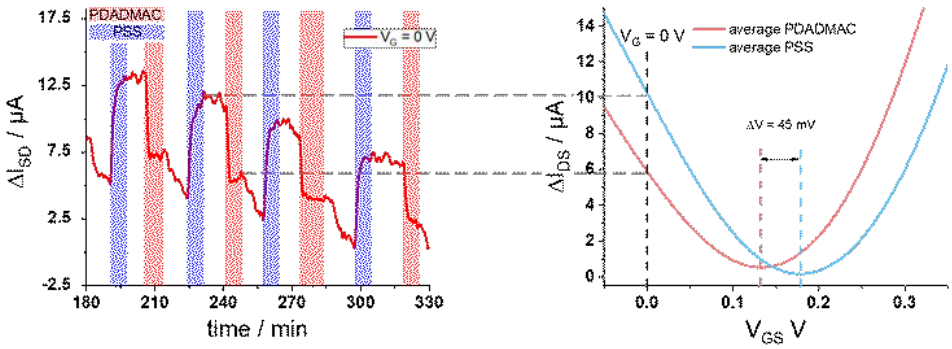

Figure S14. *left*: time resolved $I_{DS}(t)$ measurement of the LbL process and the corresponding *right*: $I_{DS}V_{GS}$ curves after layer deposition. The working point for $I_{DS}(t)$ measurements is determined by the adjusted gate voltage V_{GS} prior to the measurement.

The $I_{DS}V_{GS}$ scan cannot be observed at the same time as the $I_D(t)$ measurements, because the gate voltage needs to be modulated to record transfer characteristics, while the time-resolved measurement requires a constant gate current. Therefore, the Dirac point shift V_i is just a momentary snapshot, while $I_D(t)$ allows kinetic analysis.

- ## Voltage Drop across the PEM

The voltage drop across the PEM was calculated with the measured drain source current I_{GS} across the KCl ion solution which can be seen in Figure S15. With the initial state of the configuration, where

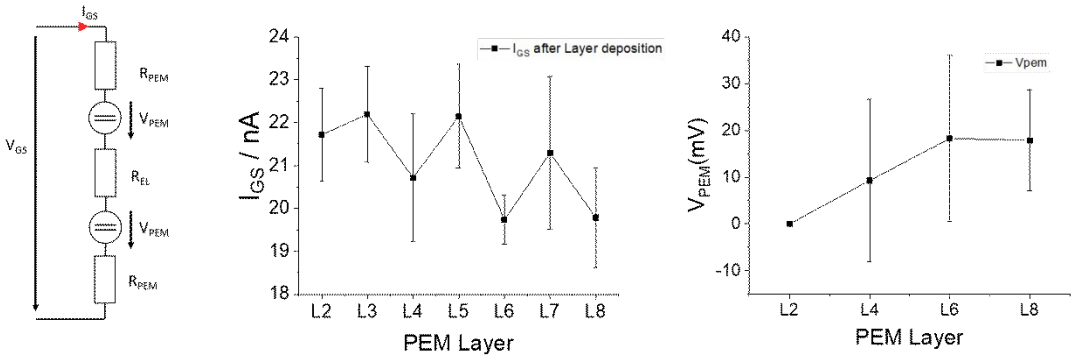

Figure S15. *left*: Electrical equivalent circuit to represent the resistance between the gate electrode and the rGO EG-FET. *middle*: The resulting gate source current $I_{GS}(t)$ after each layer deposition exemplary demonstrated at V_{GS} = + 400 mV. The total current I_{GS} variation upon layer formation is very low, but still indicates the different voltage drops across the PSS or PDADMAC layer. *right*: Voltage drop across every polyelectrolyte double layer.

RPEM = 0, the voltage drop is entirely across the electrolyte. The voltage drop after each polyelectrolyte double layer is calculated with Eq.S20.

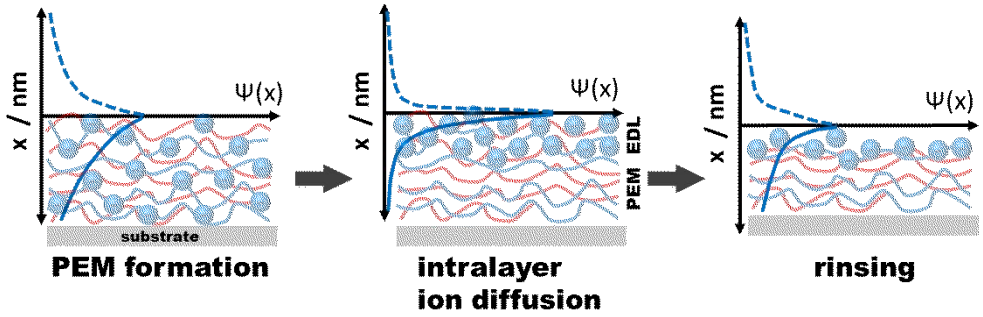

Figure S16. Surface potential Ψ as a function of the distance to the sensing surface. Upon Layer formation, surface charge density increases, hence the surface potential is modulated. The initial state after the first precursor layer are shown on the left, the adsorption of a new layer is shown in the middle and the polyelectrolyte washing off is shown in the rinsing graph.

$$V_{PEM} = V_{GS}\frac{R_{PEM}}{R_{Total}} = V_{GS}\frac{R_{PEM}}{R_{el} + 2\,R_{PEM}} \quad \text{(Eq.S20)}$$

III. Experimental procedure

- ## Preparation of the rGO-FETs

First, Micrux chips (schematically shown in Figure S17a) are sonicated in a 1 % HELMANEX(III) Milli-Q® cleaning solution for 15 minutes, then rinsed with Milli-Q®, sonicated again and finally rinsed with pure EtOH and sonicated again. The chips are then thoroughly rinsed with Milli-Q® water and put into an absolute ethanol solution with 2%v/v APTES for 1 hour. Subsequently, the chips are cleaned with absolute ethanol, gently blow dried put in an oven at 120°C for 1 hour. After cooling down to room temperature, a 12.5 µg/ml solution of graphene oxide in Milli-Q® water is drop-casted on the chips and incubated for 2 hours at room temperature. The chips are then thoroughly rinsed again with Milli-Q® water.

For the thermo-chemical reduction of the graphene oxide to reduced graphene oxide (rGO), the chips are placed into a glass petri dish with 1 ml of hydrazine monohydrate and sealed with chemically and thermally resistant Kapton tape. After 4 hours at 80°C the chips are removed from the oven, cooled to room temperature and subsequently washed with Milli-Q® water and isopropanol. Next the chips are put into a vacuum oven at 200°C for an additional thermal reduction step. After 2 hours, the rGO-FETs are controlled once again by checking the resistance before being used.

SEM images of reduced graphene oxide deposited on interdigitated electrodes to obtain a drain-source channel for FET sensors, 90 interdigitated electrode pairs with a distance of 10 µm, corresponding to a total channel width of 490 mm, can be seen in Figure S17b.

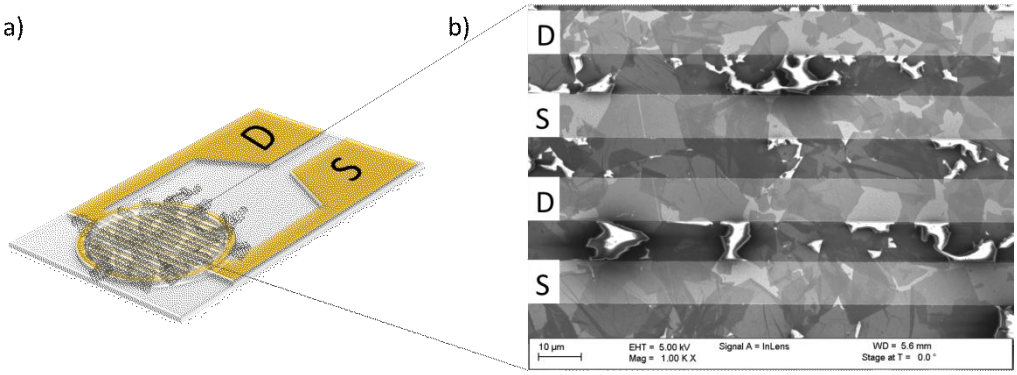

Figure S17. a) shows the glass substrate with the interdigitated electrodes, coated with reduced graphene oxide (rGO) as channel material. b) Scanning electron microscopy image of the rGO. The interdigitated electrodes have a distance of 10 µm and are alternating connected to drain and source, forming the channel of the EG-FET.

The electrical characterization of the rGO EG-FET is given by the transfer characteristic of the finalized device, shown in Figure S18. The influence on the scanning direction is shown in a slight shift of the Dirac point V_i, representing the hysteresis of the reduced graphene oxide upon field-effect probing direction.

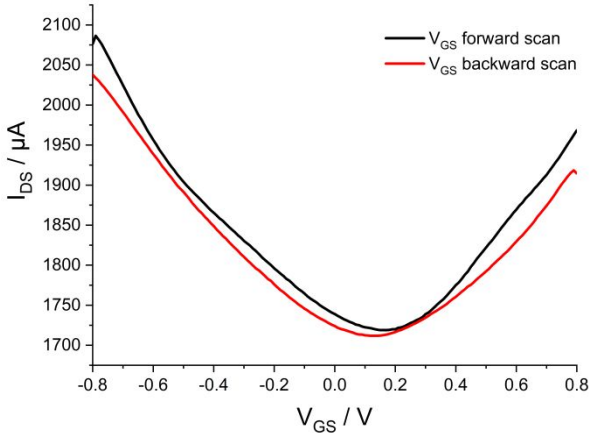

Figure S18: The transfer characteristics of the rGO EG-FET is used to characterize the sensor electrically. The drain source current I_{DS} is modulated upon applying an electric field by the gate electrode. The hysteresis of the Dirac point shift V_i upon different gate voltage V_{GS} scanning directions can be observed.

- ## Preparation of the SPR Au-slides

Standard microscope glass slides are placed into a 1% HELMANEX (III) aqueous solution and sonicated for 15 minutes. Then, the slides are cleaned with Milli-Q® water, put into pure ethanol and sonicated for an additional 15 minutes. Subsequently, the slides are placed on a slide holder which is mounted into a physical-vapor-deposition chamber. 2 nm Cr and then 50 nm Au (99.999%) are evaporated at roughly 1 x 10^{-6} mbar at evaporation rates of about 0.1 Å/s. After the evaporation, the glass slides are stored in an Argon atmosphere until being used. The slides are cut to appropriate size before measuring.

- ## Preparation of the polyelectrolyte solutions

PDADMAC and PSS solutions are prepared in concentrations of 1 mg/ml in KCl solutions with different ionic strengths (20 mM, 100 mM, 500 mM). This step is done one day before the measurement in order to give the polyelectrolytes enough time to unfold.

KCl solutions are prepared at different ionic strengths by dissolving the proper amount of KCl in Milli-Q® water.

- Experimental setup and details

For the simultaneous measurement of SPR and EG-FET the experimental setup is configured as follows:

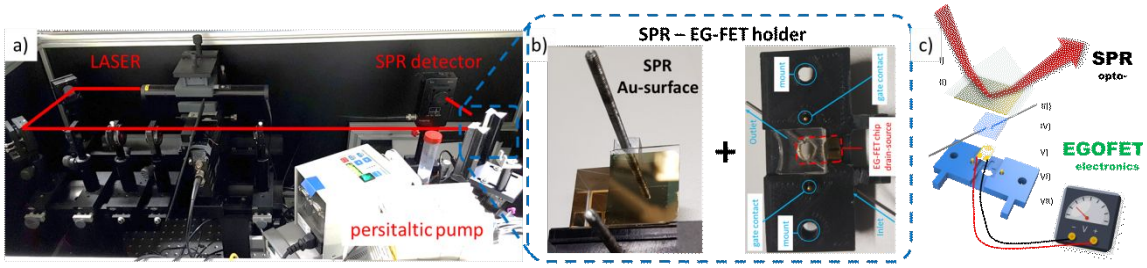

Figure S19. Experimental setup a) combined EG-FET/SPR setup, b) closeup of the EG-FET/SPR holder *left*: SPR prism with gold slide *right*: assembled microfluidic cell consisting of a PDMS-gasket, 3D printed holder, inlet and outlet, a commercial Micrux chip (IDE1) and the gate pins. c) Schematic drawing of the experimental setup consisting of the optical SPR part: I) prism II) 50 nm gold slide which also acts as the gate electrode for the electronic – EG-FET part: III) in- and outlet IV) PDMS flow cell V) interdigitated electrode chip VI) contact pins for gate electrode VII) 3D printed holder.

The SPR system in Kretschmann configuration was described in previous work.[20] Briefly, the collimated beam of a He-Ne laser (λ = 633 nm, power 10 mW), passes a linear (Glan) polarizer and a chopper before it is made incident on a prism and the reflected beam is detected using a photodiode and a lock-in amplifier. To allow for angular scans, prism and detector are mounted on a 2-circle goniometer maintaining ϑ - 2ϑ configuration. A SPR substrate, a glass slide coated with 50 nm of gold, is optically matched to the prism with immersion oil. Then, a gasket made of PDMS with flow cell with an embedded microfluidic channel as shown in Figure S20a, is placed on the SPR surface. To form a microfluidic channel, the glass substrate carrying the EG-FET channel is placed on top and pressed on to seal the flow cell. The flow cell with a channel height of 400 µm and a channel width in the sensing chamber of 3.5 mm has a volume of 5 µl (Figure S20b). The SPR surface is electrically contacted to form the gate electrode of the EG-FET.

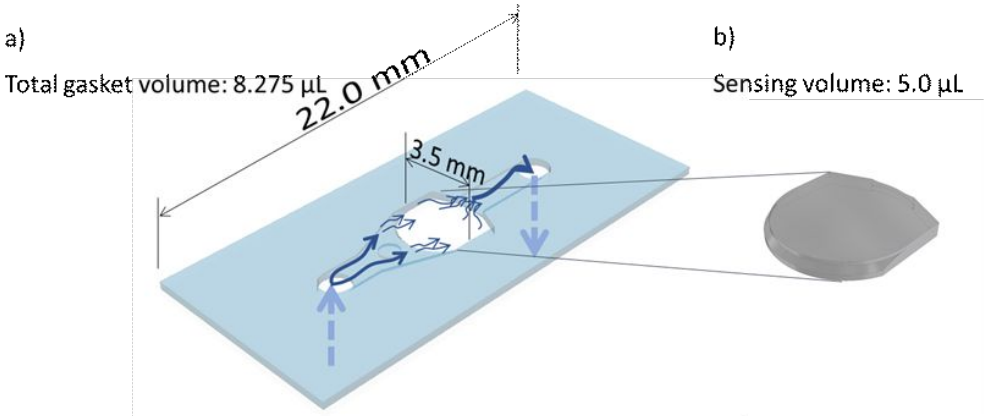

Figure S20. a) Gasket design for the SPR/EG-FET combination. The flow channel height is 400 µm, with a sensing area diameter of 3.5 mm, leading to a measurement volume of 5 µL, shown in b)

The flow cell has the following dimensions: 400 µm height, 3.5 mm diameter, 5 µL sensing volume.

- Readout software for electrical and optical measurements

Beside the development of the novel sensing platform, a software tool including a graphical user interface (GUI) was created to adjust the measurement parameters and log all measured and calculated values.

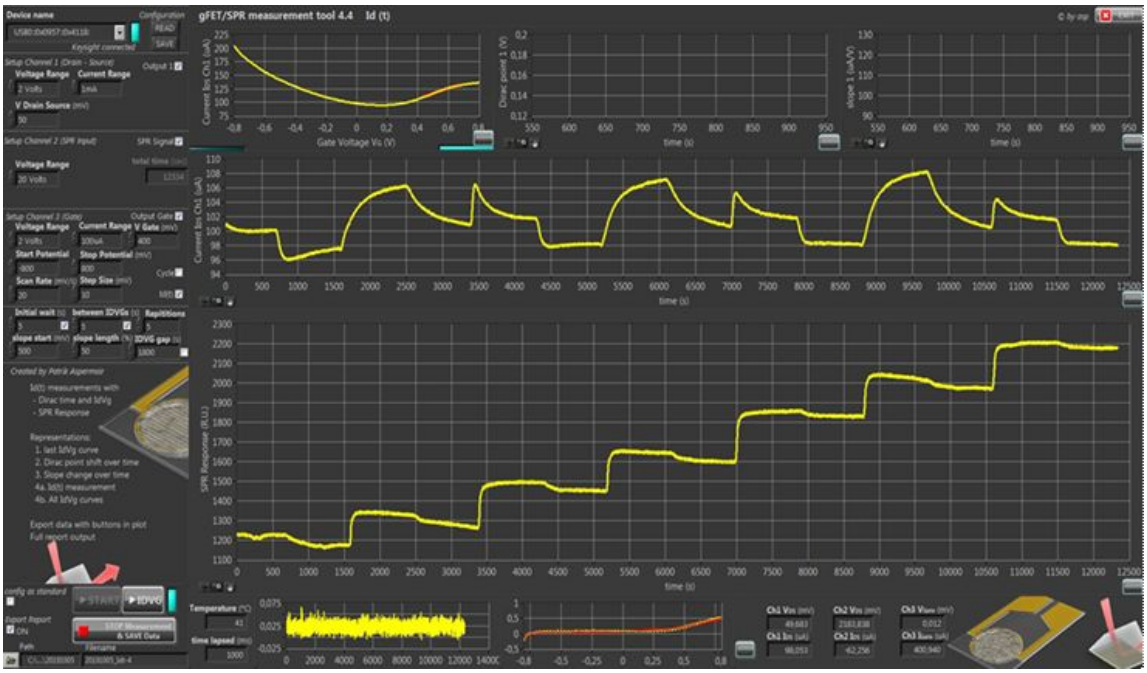

Figure S21. Layout of the measurement software. An $I_{DS}V_{GS}$ curve can be seen in the top frame, followed by a time-resolved EG-FET measurement and a time-resolved SPR measurement. The leakage current is shown at the bottom graph. All measured values are automatically exported to a spreadsheet once the measurement is finished.

IV. Materials and hardware

Hardware

BK7 glass (Hecht Assistent)
Chrome (99,9%) (MaTecK)
Metal evaporator (HHV Ltd. FL400 AUTO 306)
Gold 99,999% Au Granular 10g (MaTecK)
Multi-meter (Fluke)
U2722A USB Modular Source Measurement Unit (Keysight)
Peristaltic pump (ISMATEC ISM935C)
Molybdenum evaporation boats (HHV Ltd)
Heating oven (Thermo Scientific)
Kapton Tape (Amazon)
Tygon® 3350 tubing (ID = 0,64 mm, L = 300mm) (VWR)
Ultrasonicator ELMA S180H (Elmasonic)
Optical Microscope HR800 des Raman Systems (Horiba)
Ultimaker Cura S5 (Ultimaker)
High-refractive-index oil (Cargille Inc.)
Micrux chips IDE-1 (MicruX Technologies)
Chopper (Signal Recovery Model 197)
Lock-in amplifier (Model 5210, EG&G Princeton Applied Research)
Photodiode (ResTec)
2-circle goniometer (Huber Diffraktionstechnik)
Laser (JDS Uniphase 1125P)

Chemicals

(3-Aminopropyl)triethoxysilane (99 %, Sigma Aldrich)
Helmanex(III) solution (VWR)
Ethanol absolute (99,8 %, VWR)
Graphene Oxide Water Dispersion (0.4 wt% Concentration, Graphenea)
Hydrazine monohydrate (64-65 %, reagent grade 98 %, Sigma Aldrich)
Potassium Chloride (≥ 99 %, Sigma Aldrich)
Poly(diallyldimethylammonium chloride, PDADMAC, low molecular weight, average weight <100.000 Da, Sigma Aldrich)
Sodium 1-pyrenesulfonate (97 %. Sigma Aldrich)
Poly(sodium 4-styrenesulfonate, PSS, low molecular weight, average weight ~ 70.000 Da, Sigma Aldrich)

All chemicals and materials were used as received without further purification.

V. References

(1) Tanase, C.; Meijer, E.; Blom, P.; De Leeuw, D. Local Charge Carrier Mobility in Disordered Organic Field-Effect Transistors. *Org. Electron.* **2003**, *4* (1), 33–37.

(2) Casalini, S.; Bortolotti, C. A.; Leonardi, F.; Biscarini, F. Self-Assembled Monolayers in Organic Electronics. *Chem. Soc. Rev.* **2017**, *46* (1), 40–71.

(3) Cardon, F.; Gomes, W. On the Determination of the Flat-Band Potential of a Semiconductor in Contact with a Metal or an Electrolyte from the Mott-Schottky Plot. *J. Phys. Appl. Phys.* **1978**, *11* (4), L63.

(4) Lowe, B. M.; Skylaris, C.-K.; Green, N. G.; Shibuta, Y.; Sakata, T. Molecular Dynamics Simulation of Potentiometric Sensor Response: The Effect of Biomolecules, Surface Morphology and Surface Charge. *Nanoscale* **2018**, *10* (18), 8650–8666.

(5) Scherer, P.; Fischer, S. *Theoretical Molecular Biophysics*; Biological and Medical Physics, Biomedical Engineering; 2010.

(6) Chen, Y.; Zhang, H.; Feng, Z.; Zhang, H.; Zhang, R.; Yu, Y.; Tao, J.; Zhao, H.; Guo, W.; Pang, W.; Duan, X.; Liu, J.; Zhang, D. Chemiresistive and Gravimetric Dual-Mode Gas Sensor toward Target Recognition and Differentiation. *ACS Appl. Mater. Interfaces* **2016**, *8* (33), 21742–21749. https://doi.org/10.1021/acsami.6b02682.

(7) Macchia, E.; Picca, R. A.; Manoli, K.; Franco, C. D.; Blasi, D.; Sarcina, L.; Ditaranto, N.; Cioffi, N.; Österbacka, R.; Scamarcio, G.; Torricelli, F.; Torsi, L. About the Amplification Factors in Organic Bioelectronic Sensors. *Mater. Horiz.* **2020**, *7* (4), 999–1013. https://doi.org/10.1039/C9MH01544B.

(8) Palazzo, G.; De Tullio, D.; Magliulo, M.; Mallardi, A.; Intranuovo, F.; Mulla, M. Y.; Favia, P.; Vikholm-Lundin, I.; Torsi, L. Detection Beyond Debye's Length with an Electrolyte-Gated Organic Field-Effect Transistor. *Adv. Mater.* **2015**, *27* (5), 911–916.

(9) Macchia, E.; Manoli, K.; Holzer, B.; Franco, C. D.; Ghittorelli, M.; Torricelli, F.; Alberga, D.; Mangiatordi, G. F.; Palazzo, G.; Scamarcio, G.; Torsi, L. Single-Molecule Detection with a Millimetre-Sized Transistor. *Nat. Commun.* **2018**, *9* (1), 1–10. https://doi.org/10.1038/s41467-018-05235-z.

(10) Macchia, E.; Giordano, F.; Magliulo, M.; Palazzo, G.; Torsi, L. An Analytical Model for Bio-Electronic Organic Field-Effect Transistor Sensors. *Appl. Phys. Lett.* **2013**, *103* (10), 166_1.

(11) Manoli, K.; Magliulo, M.; Mulla, M. Y.; Singh, M.; Sabbatini, L.; Palazzo, G.; Torsi, L. Printable Bioelectronics to Investigate Functional Biological Interfaces. *Angew. Chem. Int. Ed.* **2015**, *54* (43), 12562–12576.

(12) Shirinskaya, A.; Horowitz, G.; Rivnay, J.; Malliaras, G. G.; Bonnassieux, Y. Numerical Modeling of an Organic Electrochemical Transistor. *Biosensors* **2018**, *8* (4), 103.

(13) Texas Instruments, Application Report, SLVA771, June 2016, Fu, J. *Fundamentals of On-Resistance in Load Switches*. http://www.ti.com/lit/an/slva771/slva771.pdf (accessed 2020-05-01)

(14) Kim, Y.-T.; Lee, S.; Park, S.; Lee, C. Y. Graphene Chemiresistors Modified with Functionalized Triphenylene for Highly Sensitive and Selective Detection of Dimethyl Methylphosphonate. *RSC Adv.* **2019**, *9* (58), 33976–33980.

(15) Li, M.; Liu, C.; Xie, Y.; Cao, H.; Zhao, H.; Zhang, Y. The Evolution of Surface Charge on Graphene Oxide during the Reduction and Its Application in Electroanalysis. *Carbon* **2014**, *66*, 302–311. https://doi.org/10.1016/j.carbon.2013.09.004.

(16) Kergoat, L.; Herlogsson, L.; Piro, B.; Pham, M. C.; Horowitz, G.; Crispin, X.; Berggren, M. Tuning the Threshold Voltage in Electrolyte-Gated Organic Field-Effect Transistors. *Proc. Natl. Acad. Sci.* **2012**, *109* (22), 8394–8399.

(17) Tibaldi, A.; Fillaud, L.; Anquetin, G.; Woytasik, M.; Zrig, S.; Piro, B.; Mattana, G.; Noël, V. Electrolyte-Gated Organic Field-Effect Transistors (EGOFETs) as Complementary Tools to Electrochemistry for the Study of Surface Processes. *Electrochem. Commun.* **2019**, *98*, 43–46.

(18) Eijkel, J. C.; van den Berg, A. Nanofluidics and the Chemical Potential Applied to Solvent and Solute Transport. *Chem. Soc. Rev.* **2010**, *39* (3), 957–973.

(19) Ko, Y. H.; Kim, Y. H.; Park, J.; Nam, K. T.; Park, J. H.; Yoo, P. J. Electric-Field-Assisted Layer-by-Layer Assembly of Weakly Charged Polyelectrolyte Multilayers. *Macromolecules* **2011**, *44* (8), 2866–2872.
(20) Hageneder, S.; Bauch, M.; Dostalek, J. Plasmonically Amplified Bioassay – Total Internal Reflection Fluorescence vs. Epifluorescence Geometry. *Talanta* **2016**, *156–157*, 225–231. https://doi.org/10.1016/j.talanta.2016.05.023.